Supporting Information

Improved Photovoltaic Performance of a Nonfullerene Acceptor Based on a Benzo[b]thiophene Fused End Group with Extended π-Conjugation

Kun Yang,[a,c,1] Qiaogan Liao,[a,d,1] Chang Woo Koh,[b] Jianhua Chen,[a] Mengyao Su,[a] Xin Zhou,[a] Yumin Tang,[a] Yang Wang,[a] Youming Zhang,[e] Han Young Woo,[b,*] and Xugang Guo[a,*]

[a] *Department of Materials Science and Engineering, Southern University of Science and Technology (SUSTech), No. 1088, Xueyuan Road, Shenzhen, Guangdong 518055, China*

[b] *Department of Chemistry, Korea University, Seoul 136-713, Republic of Korea*

[c] *State key Laboratory and Institute of Elemento-Organic Chemistry, Centre of Nanoscale Science and Technology and Key Laboratory of Functional Polymer Materials, College of Chemistry, Nankai University, Tianjin 300071, China*

[d] *School of Materials Science and Engineering, Harbin Institute of Technology, Harbin 150001, China*

[e] *Key Laboratory of Optoelectronic Devices and Systems of Ministry of Education and Guangdong Province, College of Optoelectronic Engineering, Shenzhen University, Shenzhen, 518060, China*

* To whom correspondence should be addressed.

Email: hywoo@korea.ac.kr (H. Y. W.); guoxg@sustc.edu.cn (X.G.)

Table of Content

1. Experimental Section.

1.1 Materials Synthesis. All reactions were carried out under argon atmosphere using Schlenk line technique unless otherwise stated. The anhydrous solvents were distilled according to the standard protocols. All the chemicals, including the starting materials benzo[b]thiophene-2-carboxylic acid (**1)** and IT-CHO (**4)**, were purchased from commercial suppliers and used without further purification.

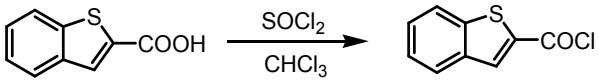

1 **2**

Synthesis of benzo[b]thiophene-2-carbonyl chloride (**2**).[1] To a solution of compound **1** (4.8 g, 27 mmol) in 50 mL dry chloroform and 1 mL DMF, 13 g thionyl chloride (7.2 mL, 13.2 mmol) was added dropwise under nitrogen. Upon the completion of addition, the reaction mixture was heated at 65 ^{o}C for 1 h before cooled down. After the removal of the unreacted thionyl chloride and solvent, the crude product **2** was obtained as a yellow residue, which was used for next step without further characterization and purification.

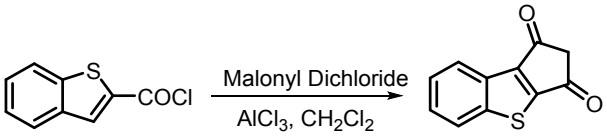

2 **3**

Synthesis of 1H-benzo[b]cyclopenta[d]thiophene-1,3(2H)-dione **(3)**. To a flask was charged with a solution of malonyl dichloride (11.7 mL, 12.0 mmol) and 21.7 g $AlCl_3$

(16.3 mmol) in CH_2Cl_2, a solution of compound **2** in 20 mL dry CH_2Cl_2 was slowly added in an ice bath. After stirring at 65 °C for overnight under nitrogen, the reaction mixture was cooled down and poured into a 10% (w/w) aqueous solution of oxalic acid slowly at 0 °C. To the solution was then added a $NaHCO_3$ solution with care until the pH was close to 7, which was followed by an extraction with dichloromethane three times. The combined organic phase was dried over Na_2SO_4 and rot-evaporated to give a residue, which was purified with column chromatography on silica gel using CH_2Cl_2 as the eluent to afford the final product as a yellow solid (2.0 g, 37%). ^{1}H NMR (400 MHz, $CDCl_3$) δ (ppm): 8.37 (d, 5.22 Hz, 1H), 7.96 (d, J = 5.90 Hz, 1H), 7.60-7.58 (m, 2H), 3.52 (s, 2H). ^{13}C NMR (100 MHz, $CDCl_3$) δ (ppm): 190.30, 190.02, 157.92, 152.68, 148.08, 130.39, 129.26, 127.13, 125.98, 124.08, 49.13. HR-MS (ESI): calcd for $C_{11}H_6O_2S$, 202.0089; found: 202.0163.

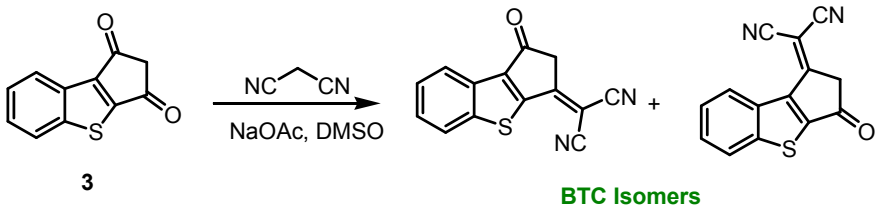

3 **BTC Isomers**

Synthesis of 2-(3-oxo-2,3-dihydro-1H-benzo[b]cyclopenta[d]thiophen-1-ylidene) malononitrile and 2-(1-oxo-1,2-dihydro-3H-benzo[b]cyclopenta[d] thiophen-3-ylidene)malononitrile **(BTC Isomers)**. To a solution of 500 mg compound **3** (2.5 mmol) and malononitrile (231 mg, 3.5 mmol) in 15 mL anhydrous dimethyl sulfoxide, 287 mg anhydrous sodium acetate (287 mg, 3.5 mmol) was added. The reaction was changed to purple color soon and stirred at room temperature for 1 h. Then, the reaction mixture was poured into water and acidified with HCl solution to a pH of 1-2. The

precipitate was filtered and then purified by column chromatography using dichloromethane as the eluent to give a greenish solid as the product (463 mg, 68%). ^{1}H NMR (400 MHz, $CDCl_3$) δ (ppm): 8.41 (d, J = 7.15 Hz, 1H), 8.02 (d, J = 7.97 Hz, 1H), 7.70-7.63 (m, 2H), 4.00 (s, 2H). ^{13}C NMR (100 MHz, $CDCl_3$) δ (ppm): 187.72, 162.17, 157.28, 148.93, 148.50, 130.27, 127.83. 127.70, 125.72, 123.88, 111.81, 111.52, 46.32. HR-MS (ESI): calcd for $C_{14}H_6N_2OS_2$, 250.0210; found: 250.0245.

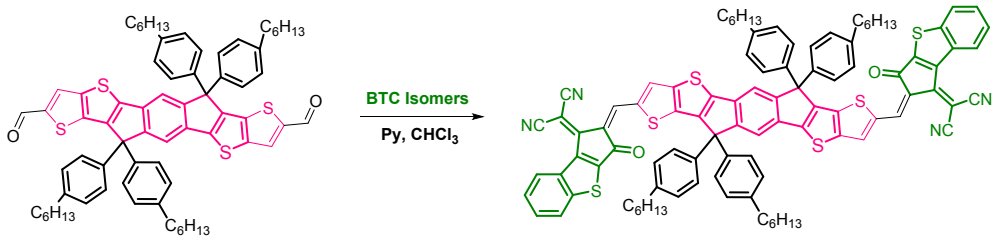

Synthesis of ***ITBTC*** (**5**). To a solution of 100 mg (0.093 mmol) ITT-CHO in 10 mL chloroform was added TTC (232 mg, 0.93 mmol) and 1 mL pyridine. The reaction mixture was kept at 90 °C for overnight and then precipitated into 100 mL methanol upon cooled down. The precipitate was filtered and then purified with column chromatography over silica gel using chloroform as the eluent to give a deep blue solid as the product (87 mg, 61%).^{1}H NMR (400 MHz, $CDCl_3$) δ (ppm): 8.60 (s, 2H), 8.46-8.43 (m, 2H), 8.23 (s, 2H), 7.97-7.95 (m, 2H), 7.85 (s, 2H), 7.83-7.80 (m, 4H), 7.25 (d, J = 7.91 Hz, 8 H), 7.19 (d, J = 9.71 Hz, 8H), 2.60 (t, J = 8.0 Hz, 8H), 1.39-1.25 (m, 24H), 0.91-0.85 (m, 12H). ^{13}C NMR (100 MHz, $CDCl_3$) δ (ppm): 182.51, 157.64, 155.31, 154.79, 154.51, 147.43, 147.38, 145.72, 143.98, 143.29, 142.45, 139.17, 138.39, 136.77, 135.50, 135.04, 130.31, 129.41, 128.92, 128.87, 127.94, 127.35, 125.17, 124.94, 123.67, 118.33, 114.00, 113.49, 69.27, 63.25, 35.64, 31.72, 31.30,

29.22, 22.61, 14.21. HR-MS (ESI): calcd for $C_{98}H_{82}N_4O_2S_6$, 1538.4762; found: 1538.4810. Elemental Analysis: C, 76.43; H, 5.37; N, 3.64, Found: C, 76.11; H, 5.77; N, 3.39.

1.2 Materials Characterization.

The ^1H and ^{13}C NMR spectra of compounds were recorded on a Bruker Ascend 400 MHz spectrometer. Elemental analyses (EAs) of ITBTC were performed on Vario EL Cube at Shenzhen University (Shenzhen, Guangdong). Thermogravimetric analysis (TGA) curves were recorded on a Mettler, STARe TA Instrument. UV-Vis absorption spectra were recorded on a Shimadzu UV-3600 UV-VIS-NIR spectrophotometer. Cyclic voltammetry (CV) measurements were carried out using a CHI760E voltammetric analyzer with 0.1 M tetra(*n*-butyl)ammonium hexafluorophosphate (Bu_4NPF_6) in acetonitrile as the supporting electrolyte. A platinum disk, platinum wire, and silver wire were employed as the working electrode, counter electrode, and reference electrode, respectively. The scan rate was 100 mV s^{-1}, and Fc/Fc^+ redox couple was used as the internal reference for all measurements. AFM measurements of pure acceptor films and blend films were performed by using a Dimension Icon Scanning Probe Microscope (Asylum Research, MFP-3D-Stand Alone) in tapping mode. All the TEM measurements were carried out on a Tecnai Spirit microscopy (20 kV) with the samples prepared by casting the films on PEDOT:PSS covered substrates firstly followed by floating off in deionized water before being transferred onto a TEM copper grids.

1.3 GIXD Measurements.

Two-dimensional grazing incident wide-angle X-ray scattering (2D GIWAXD) measurements were performed at the 9A beamline in the Pohang Accelerator Laboratory (PAL), Pohang Korea. The energy, pixel size, wavelength, and scanning interval at the 9A beamline were 11.075 keV, 79.59 μm, 1.11946 Å, and 2θ = 0°–20°, respectively. The scattering vectors, q_{xy} and q_z were respectively parallel and perpendicular to the substrate. The acceptors and their blend films were prepared on Si substrates using identical spin speeds, solvents, concentrations, and annealing temperatures and times as for the relevant OSC devices. All scattering images were collected in air. The films were exposed for 20 sec. To account for the gaps in the detector array, two images were taken per sample, one with the detector in the standard position and the other translated 23 mm down to fill the gap, the two images are then merged. 1D linecuts were taken from the 2D scattering spectra in the in-plane and out-of-plane directions using the GIXSGUI software package developed by the beamline scientists. To account for air scatter, the linecuts were background subtracted utilizing an exponential fit. The background-subtracted peaks were fit using the multipeak fit function in Igor Pro. Scherrer analysis was performed utilizing the method developed by Smiglies to account for instrumental broadening and detection limits in the 2D detector. The values presented represent a lower limit for correlation length since the Scherrer analysis does not account for broadening due to defects in the crystallites.

1.4 Device Fabrication Procedures.

Organic Solar Cells. The indium tin oxide (ITO)-coated glass substrates (10

ohms/square) were cleaned through ultrasonic treatment in detergent, DI water, acetone, and isopropyl alcohol and then dried in an oven overnight. PEDOT:PSS (Clevios P VP A1 4083) (~30 nm) was spin-coated (3000 rpm/30 s) onto ultraviolet ozone-treated ITO substrates. After annealing at 150 °C for 10 min. in air, the substrates were transferred into a N_2 glovebox. The CB solution stirred at 80 ºC overnight (an overall concentration of 16 mg/mL; D:A=1:1 wt ratio) was spin-coated on top of the PEDOT:PSS layer with or without additive. The blend film thickness was controlled at ~110 nm, measured by KLA-TENCOR Alpha-Step Surface Profiler. Then, the blend films were annealed at 100 ^{o}C for 10 min. PDINO (perylene diimide functionalized with amino N-oxide) in ethanol solution (1.0 mg/mL) was spin-coated on top of active layer to form a cathode buffer layer. Finally, 100 nm Al cathode was deposited (area 4.5 mm^2 defined by metal shadow mask) on the active layer under a high vacuum (1×10^{-4} Pa) using a thermal evaporator. For device characterization, all current-voltage (*I-V)* characteristics of the devices were measured under simulated AM1.5G irradiation (100 mW/cm^2) using a Xe lamp-based SS-F5-3A Solar Simulator (Enli Technology, Inc.). A Xe lamp equipped with an AM1.5G filter was used as the white light source. The light intensity was controlled with an NREL-calibrated Si solar cell with a KG-5 filter. The external quantum efficiency (EQE) was measured by a QE-R3011 measurement system (Enli Technology, Inc.).

1.5 SCLC Mobility Measurements. Hole and electron mobilities were measured using the space charge limited current (SCLC) method. The structure of ITO/PEDOT:PSS/ PBDB-T:ITBTC/MoO_3/Ag was used for hole-only devices and the structure of ITO/

ZnO/PBDB-T:ITBTC/PFN/Al was used for electron-only devices, respectively. The SCLC mobilities were calculated based on the MOTT-Gurney equation:[2]

$$J = \frac{9}{8}\varepsilon_0\varepsilon_r\mu\frac{V^2}{d^3}$$

Where J is the current density, ε_r is the relative dielectric constant of active layer usually with a value of 2-4 for organic semiconductors, herein we use a relative dielectric constant of 3 for polymer, ε_0 is the permittivity of empty space, μ is the mobility of hole or electron and d is the thickness of the active layer, V is the internal voltage in the device, and $V = V_{appl} - V_{bi}$, where V_{appl} is the voltage applied to the device, and V_{bi} is the built-in voltage resulting from the relative work function difference between the two electrodes (in the hole-only and the electron-only devices, the V_{bi} values can be neglected).

2. Representative IC-Based End Groups Reported in Literature.

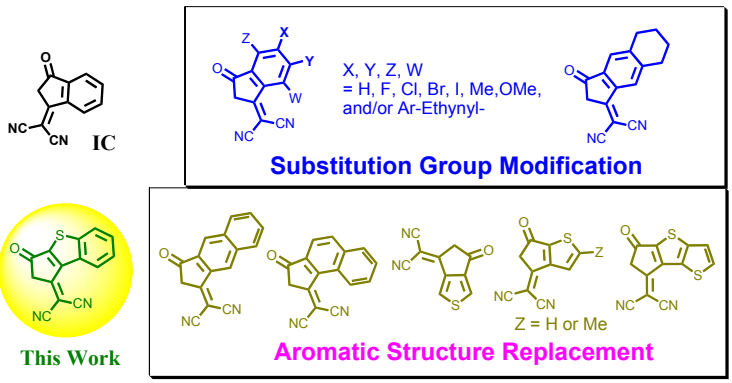

Scheme S1. The representative 2-(3-oxo-2,3-dihydroinden-1-ylidene) malononitrile (IC)-based end groups reported in literature together with the new end group designed in this work. Currently most of IC-based end groups are built by either modifying the phenyl ring substitution groups or replacing phenyl moiety with other aromatic structures.[3-6]

3. Thermal Properties of ITBTC.

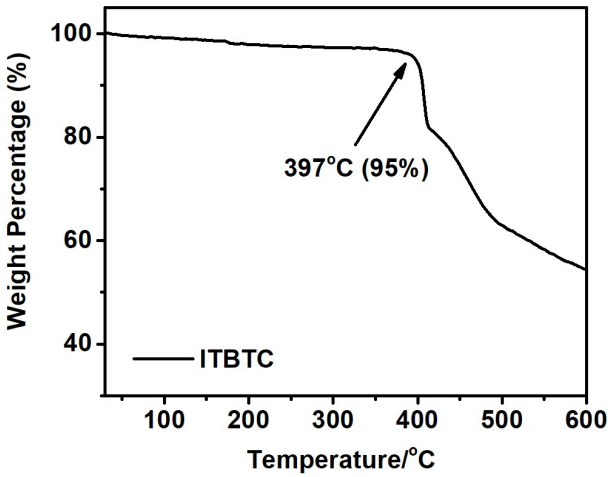

Figure S1. Thermal gravimetric analysis (TGA) curves for ITBTC, heating rate: 10 ^{o}C/min in nitrogen atmosphere.

4. CV Curves and Optoelectronic Properties of ITBTC and ITIC.

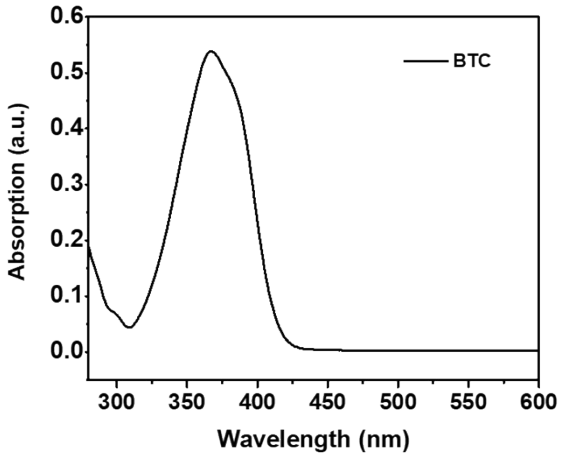

Figure S2. UV-Vis absorption spectrum of BTC end group in chloroform solution.

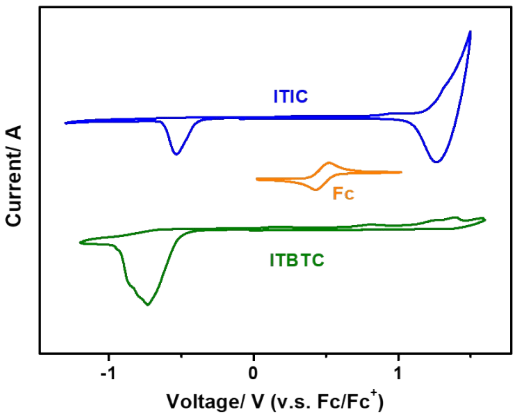

Figure S3. Cyclic voltammetry of ITBTC and ITIC measured under the same conditions using 0.1 M tetra(*n*-butyl)ammonium hexafluorophosphate (Bu_4NPF_6) in acetonitrile as the supporting electrolyte with a platinum disk, platinum wire, and silver wire serving as working electrode, counter electrode, and reference electrode, respectively. The scan rate was 100 mV s^{-1} and Fc/Fc^+ was used as the reference for all measurements.

Table S1. Summary of optoelectronic properties of ITBTC and ITIC.

Material	λ_{max} CF/nm	λ_{max} Film/nm	λ_{onset} Film/nm	$E_{g\,opt}$ (eV) [a]	E_{HOMO} (eV)[b]	E_{LUMO} (eV)[b]	$E_{g\,b}$ (eV)
ITBTC	661	686	768	1.61	-5.38	-3.78	1.6
ITIC	665	711	775	1.60	-5.48	-3.90	1.58

a) Calculated based on the equation: $E_g = 1240/\lambda_{onset\ of\ Film}$; b) extracted from cyclic voltammetry curves.

5. Photovoltaic Performance of PBDB-T:Small Molecule Acceptor-Based Solar Cell Devices.

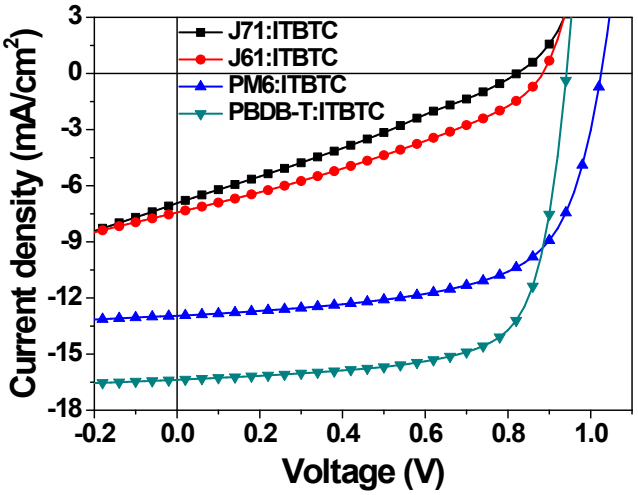

Figure S4. *J-V* curves for the solar cells based on ITBTC blended with different donor materials.

Table S2. Photovoltaic performance parameters for the solar cells based on different donor materials.

Donor	V_{oc} (V)	J_{sc} (mA cm^{-2})	FF (%)	PCE_{max} (%)
J61	0.883	7.43	33.5	2.20 (1.98 ± 0.32)
J71	0.821	6.93	28.3	1.61 (1.35 ± 0.46)
PM6	1.030	12.96	64.0	8.51 (8.32 ± 0.22)
PBDB-T	0.941	16.37	71.3	10.99 (10.77 ± 0.25)

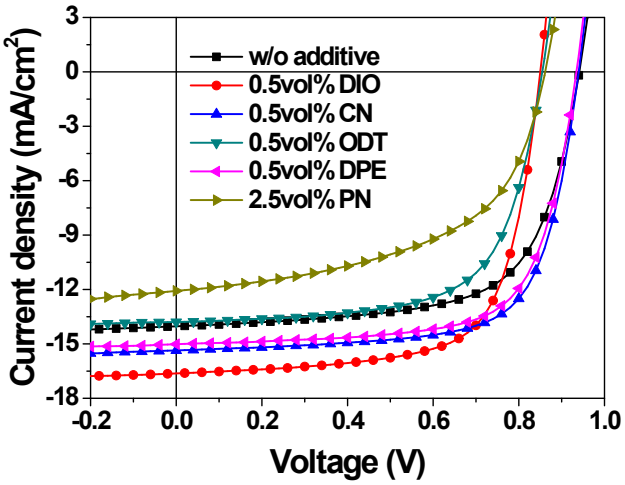

Figure S5 *J-V* curves for solar cells based on PBDB-T:ITBTC blend fabricated with different additives.

Table S3. Photovoltaic performance parameters for PBDB-T:ITBTC solar cells based on different additives.

Additive	V_{oc} (V)	J_{sc} (mA cm^{-2})	FF (%)	PCE_{max} (%)
w/o	0.941	14.03	65.9	8.71 (8.63 ± 0.28)
0.5 vol% DIO	0.849	16.89	69.1	9.90 (9.77 ± 0.17)
0.5 vol% CN	0.940	15.36	70.3	10.14 (9.79 ± 0.36)
0.5 vol% ODT	0.849	14.75	64.0	8.04 (7.82 ± 0.29)
0.5 vol% DPE	0.934	15.01	69.9	9.80 (9.76 ± 0.31)
2.5 vol% PN	0.870	12.89	57.8	6.48 (5.81 ± 0.77)

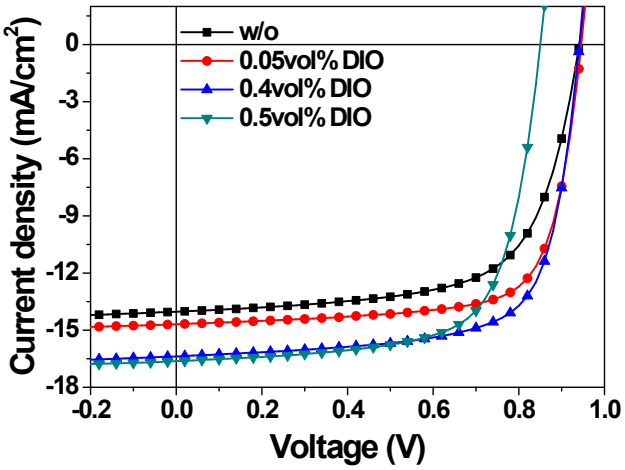

Figure S6. *J-V* curves for solar cells based on PBDB-T:ITBTC blend fabricated with different content of DIO.

Table S4. Photovoltaic performance parameters for PBDB-T:ITBTC solar cells based on different content of DIO as the processing additive.

DIO content (vol%)	V_{oc} (V)	J_{sc} (mA cm^{-2})	FF (%)	PCE (%)
w/o	0.941	14.03	65.9	8.71 (8.63 ± 0.13)
0.05	0.945	14.69	73.2	10.17 (9.87 ± 0.39)
0.4	0.941	16.37	71.3	10.99 (10.77 ±0.25)
0.5	0.849	16.89	69.1	9.90 (9.77 ± 0.33)

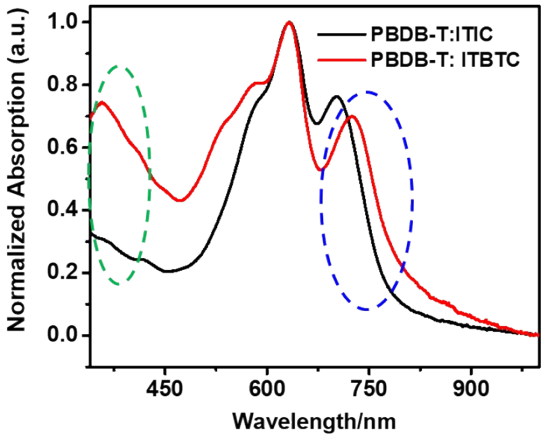

Figure S7. UV-Vis absorption spectra of PBDB-T:ITBTC and PBDB-T:ITIC blend films. The stronger absorption of the PBDB-T:ITBTC blend film at the 350-450 nm range (green dash circle) should be responsible for the higher EQE response of the ITBTC-based devices in the corresponding ranges (Figure 3b). Similar result was observed in the long wavelength range (blue dash circle), which should be responsible for the slightly red-shifted EQE edge of ITBTC-based devices.

6. Hole and Electron Mobilities and Photoluminescence (PL) Spectra of PBDB-T:Small Molecule Acceptor Blend Films.

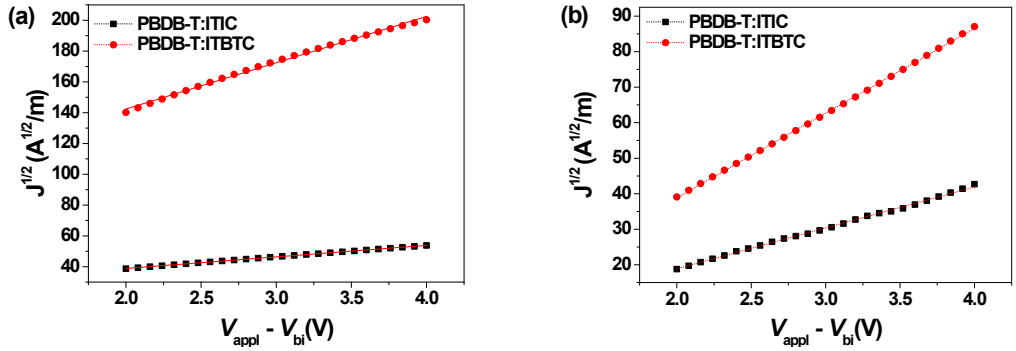

Figure S8. The corresponding $J^{1/2}$–V curves for the hole-only (a) and electron-only (b) devices based on the PBDB-T:ITIC and PBDB-T:ITBTC blend film (in dark), respectively. The films were prepared under the same condition for the optimal solar cells.

Table S5. The charge transport properties of ITBTC measured from SCLC method.

Blend film	μ_h (cm^2 V^{-1} s^{-1})	μ_e (cm^2 V^{-1} s^{-1})	μ_h/μ_e
PBDB-T:ITIC	$(7.13 \pm 0.22) \times 10^{-5}$	$(1.32 \pm 0.24) \times 10^{-5}$	5.40
PBDB-T:ITBTC	$(1.32 \pm 0.10) \times 10^{-4}$	$(8.66 \pm 1.10) \times 10^{-5}$	1.52

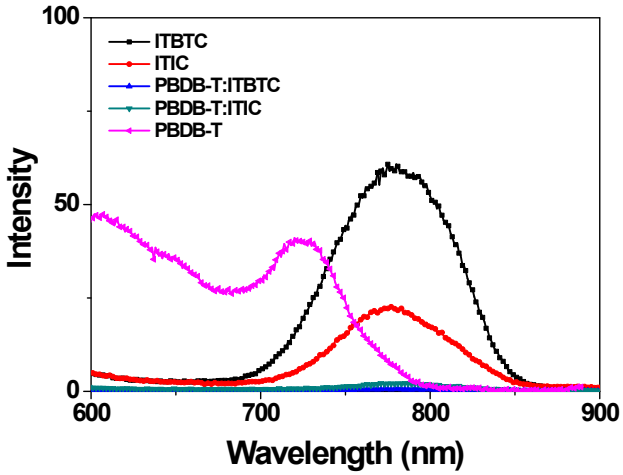

Figure S9. PL spectra of ITBTC, ITIC neat films, and PBDB-T:ITBTC, PBDB-T:ITIC blend films (excited at 500 nm).

7. DSC Curves of ITIC, ITBTC and Their Blend Film with PBDB-T.

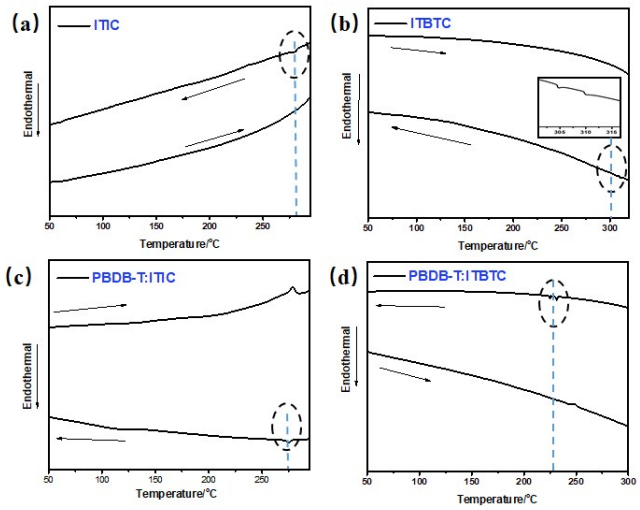

Figure S10. DSC curves of ITIC (a), ITBTC (b), and their blends with polymer PBDB-T (c, d). The relatively larger shift of crystallization transition peaks for ITBTC after blended with PBDB-T indicated a better intermixing of the new acceptor ITBTC with the polymer in the blend phase, likely due to the possible formation of extra S···S interactions between the BTC end group with the thiophene moiety in polymer.

8. 2D-GIWAXS Linecut Profiles of Films.

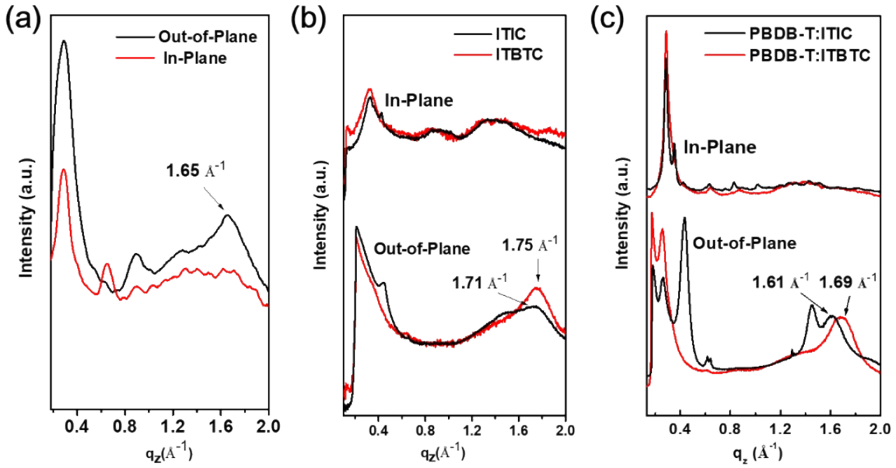

Figure S11. The in-plane and out-of-plane linecut profiles of GIWAXS of the (a) PBDB-T film and (b) the neat films and (c) blend films of PBDB-T:ITIC (black) and PBDB-T:ITBTC (red).

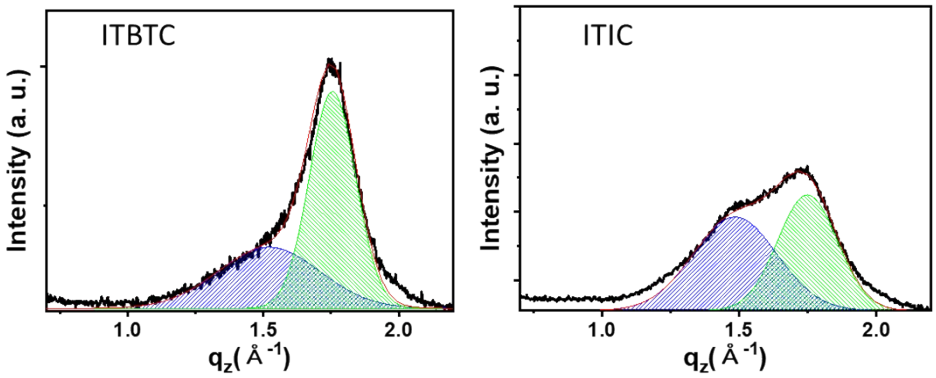

Figure S12. The deconvoluted diffraction peaks of ITBTC and ITIC films in the OOP directions via multipeak fitting process. The corresponded π-π stacking distance and related data of these films are summarized in Table S6.

Table S6. Packing parameters for the pure and blending films of ITBTC and ITIC based on the GIWAXS measurements.

Pristine films	peak	q (Å^{-1})	d-spacing (Å)	FWHM (Å^{-1})	CCL_{010} (Å)	Ratio of area (%)	Area
ITBTC	low q	1.521	4.1	0.441	12.9	38.2	51.7
	high q	1.755	3.6	0.202	28.3	61.8	83.6
ITIC	low q	1.485	4.2	0.358	15.9	53.2	260
	high q	1.749	3.6	0.255	22.4	46.8	229

9. ^{1}H and ^{13}C NMR spectra of Compounds.

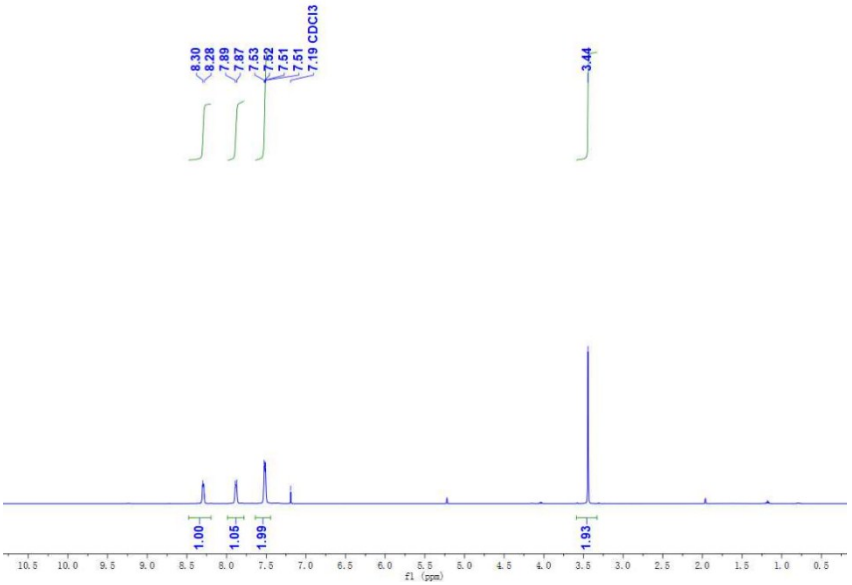

Figure S10. ^{1}H NMR spectrum of Compound **3**.

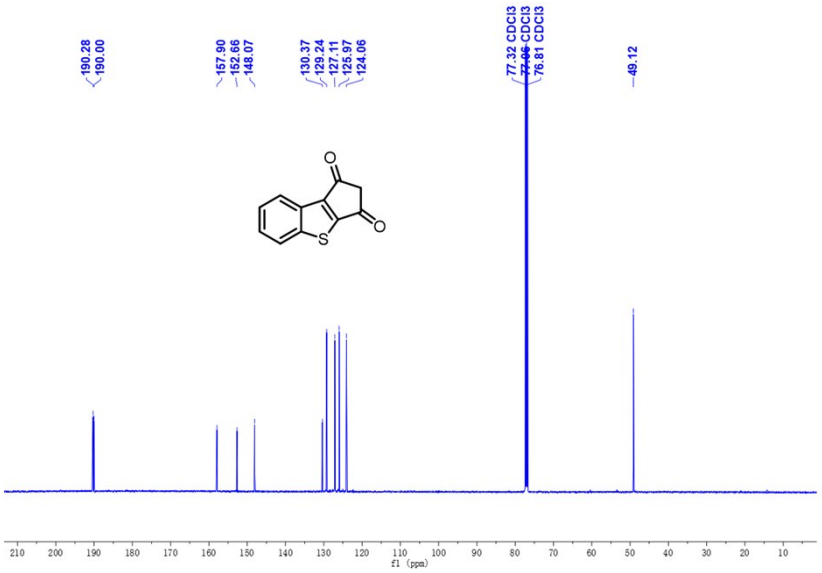

Figure S11. ^{13}C NMR spectrum of Compound **3**.

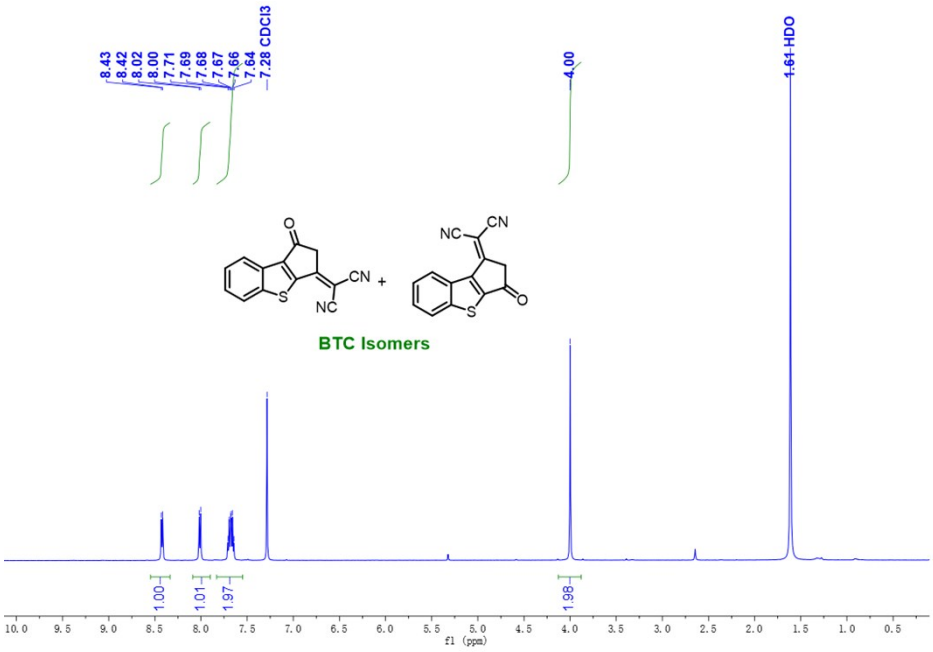

Figure S12. ^{1}H NMR spectrum of Compound **BTC**.

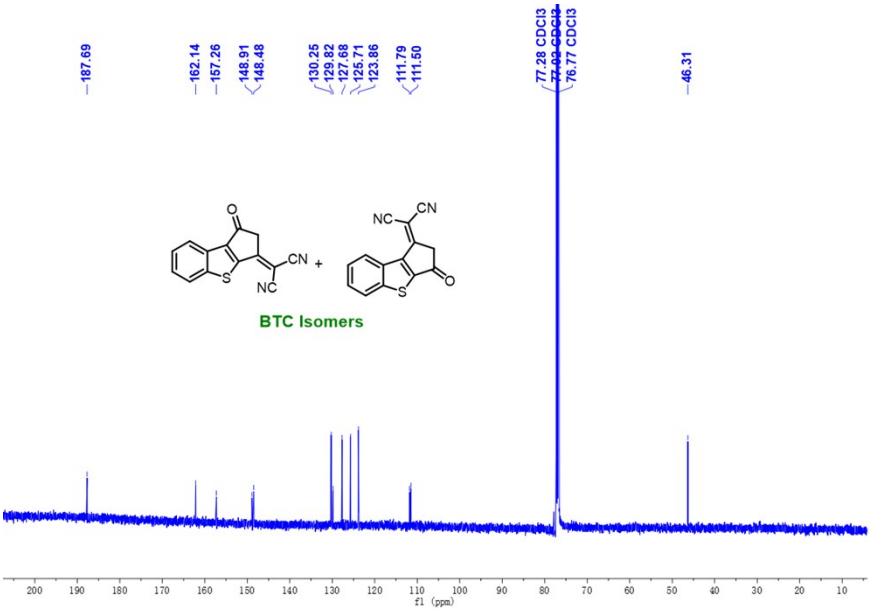

Figure S13. ^{13}C NMR spectrum of Compound **BTC.**

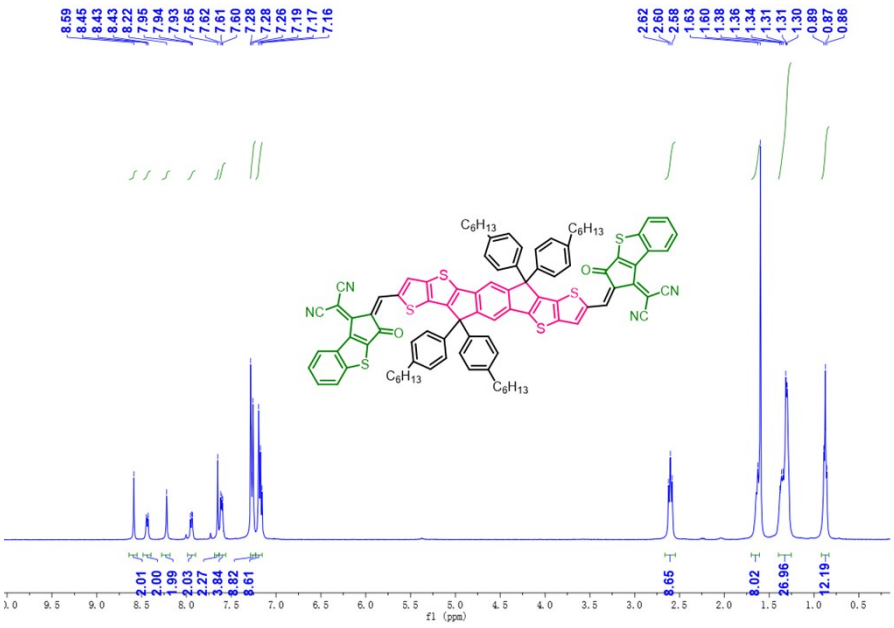

Figure S14. ^{1}H NMR spectrum of Compound **ITBTC.**

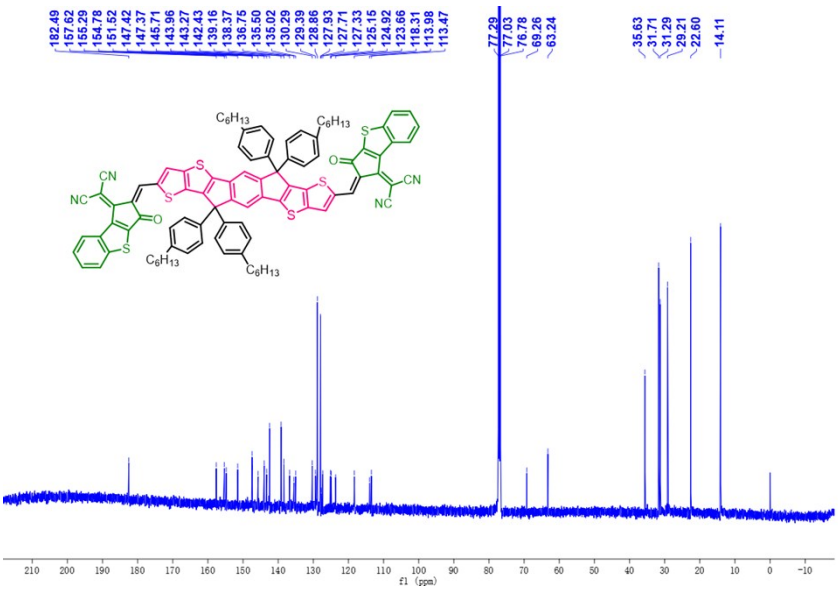

Figure S15. ^{13}C NMR spectrum of Compound **ITBTC.**

References

1. S.-L. Chang, F.-Y. Cao, W.-C. Huang, P.-K. Huang, K.-H. Huang, C.-S. Hsu and Y.-J. Cheng, *ACS Energy Lett.*, 2018, **3**, 1722-1729.
2. R. Steyrleuthner, M. Schubert, F. Jaiser, J. C. Blakesley, Z. Chen, A. Facchetti and D. Neher, *Adv. Mater*. 2010, **22**, 2799-2803.
3. F. Shen, J. Xu, X. Li and C. Zhan, *J. Mater. Chem. A*, 2018, **6**, 15433-15455.
4. R. Yu, H. Yao, L. Hong, Y. Xu, B. Gao, J. Zhu, Y. Zu and J. Hou, *Adv. Energy Mater.* 2018, **30**, 1802131.
5. F. Yang, C. Li, W. Lai, A. Zhang, H. Huang and W. Li, *Mater. Chem. Front.*, 2017, **1**, 1389-1395.
6. S. M. Swick, W. Zhu, M. Matta, T. J. Aldrich, A. Harbuzaru, J. T. Lopez Navarrete, R. Ponce Ortiz, K. L. Kohlstedt, G. C. Schatz, A. Facchetti, F. S. Melkonyan and T. J. Marks, *Proc. Natl. Acad. Sci. U.S.A.* 2018, **115**, 8341-8348.